Main Manuscript for

Enhancing the localization precision of single molecule localization microscopy by analyzing Brownian motion of individual fluorescent probe

Jielei Ni [a, 1], Bo Cao [a, 1], Gang Niu [b], Chen Xu [a], Yanxiang Ni [a, 2],

[a] Nanophotonics Research Center, Shenzhen Key Laboratory of Micro-Scale Optical Information Technology & Institute of Microscale Optoelectronics, College of Physics and Optoelectronic Engineering, College of Electronics and Information Engineering, Shenzhen University, Shenzhen, China

[b] PhilRivers Technology, Beijing, China

[1] J. N. and B. C. contributed equally to this work

[2] To whom correspondence should be addressed. **Email:** niyanxiang0000@gmail.com

Abstract

The localization precision is a crucial parameter for single-molecule localization microscopy which directly influences the achievable spatial resolution. Although extensive studies have been conducted showing localization precision can be influenced by experimental factors such as photon number, noise, pixelation, sample drift, etc., less attention has been paid to the influence of Brownian motion of fluorescent probes in imaging buffer. Here we address this issue and provide a statistical method to analyze the motion of fluorescent probes. By calculating the significance of displacement between different frames, evidence of Brownian motion was provided. Its influence on localization precision was also discussed. Out results provide new insight into the optimization of localization precision for researchers using super-resolution localization microscopy.

Introduction

Single-molecule localization microscopy (SMLM) such as stochastic optical reconstruction microscopy (STORM) (1), photo-activated localization microscopy (PALM) (2), DNA-PAINT (3) or MINFLUX (4-6) has circumvented the diffraction barrier, offering 2-30 nm lateral resolution and the possibility of 3D imaging (1-8). SMLM has allowed for unprecedented high-resolution visualization of various biological structures such as microtubules, actin, clathrin-coated pits, mitochondria, chromatin complexes, neurons, ER, and focal adhesion complexes, which are previously considered impossible due to the diffraction limit (9).

In SMLM, fluorophores can be temporally separated, so that a sparse set of emitters is captured in one camera frame, to avoid spatial overlap of their point spread functions (PSF). The temporal separation of the fluorophores can be achieved via photoactivation (2), stochastic switching of fluorophores between a fluorescent and nonfluorescent state (1), or the reversible binding of fluorophore to the target site (3). The sparse set of activated fluorophores in each frame is then localized by fitting Gaussians to individual intensity peaks. These detected peaks can then be grouped over space and time to precisely estimate the location of the individual emitters, forming a high-resolution image. Experimental factors, such as the number of photons collected at each point, pixelation of the detector and noise sources in the detection process including shot noise of the photons, background noise created by out-of-focus fluorescence, readout noise and dark current of detector, will influence the localization precision. Theoretical calculation of the best localization precision is given by the square root of the Cramér-Rao lower bound (CRLB) based on a statistical theory concerning the Fisher information matrix. Analytical expressions are also given to show how the localization error can be reduced by experimental conditions [10-11].

Although localization error can be minimized by optimizing experiment conditions using the above-mentioned theoretical model, it is still hard to reach its theoretical limit. There are many factors that could cause the discrepancy such as optical aberration and sample motion. Sample or instrument drift during acquisition is one common type of sample motion. Drift caused by temperature changes or mechanical relaxation effects can occur in the range of several hundred nanometers over the course of a few minutes. Approaches for drift compensation have been proposed including reference markers (1, 12-13) and cross-correlation correction (14-15) in the past years. The influence of drift can be minimized by these methods, but is generally unavoidable.

Brownian motion of the fluorescent probe is another type of sample motion that is unfortunately impossible to be corrected due to its unpredictable trajectory. The influence of Brownian motion to localization precision has been reported in the measurement of the diffusion coefficient by single particle tracking (SPT). It is shown that Brownian motion during imaging process can lead to distortion of the shape of the observed intensity distribution, resulting in a deterioration of the localization precision compared to the stationary one (16-17). In SMLM experiments where fluorescent DNA probes are widely used (18-21), fluorescent dye labelled on the free end of the DNA would exhibit random walk similar to that of Brownian particles, except that the domain is restricted by the DNA strand. Although the influence of label displacement on resolution has been reported (11), the Brownian motion of DNA probes and its influence of localization precision has not been studied by far.

Here, we present a statistical method for the analysis of the molecule motion of fluorescent probes.

Z-score was introduced to define the statistically significant difference between displacement of two localizations from adjacent frames and that from random frames. Molecules with large negative z-score were analyzed, revealing the existence of Brownian motion. The deterioration of Brownian motion on localization precision was demonstrated. Different from the drift compensation approaches that correct the collective motion of molecules, our results reveal the possibility of improving localization precision by recognition of the motion of single molecule.

Results and discussion

Physical picture for Brownian motion of fluorescent DNA probes in STORM imaging

Fluorescently labelled DNA probes are widely used in STORM imaging because their suitability for the attachment of single dye or pairs of photoswitchable dyes with designable length.

To demonstrate the Brownian motion of fluorescent probes, we used single-strand DNAs with 18 nucleotides immobilized to a glass surface. Alexa Fluor 647 was attached to the 3' end of the DNA strand. Since the fixed point of the DNA to the glass surface is non-selected, the DNA probes have various tether length R, as illustrated in Fig. 1a. The DNA strand can coil up in imaging buffer in a random fashion, so that the position of the dye changes with time. This is closely analogous to the Brownian motion of the dye within a domain confined by the tether length.

Fig. 1b depicts the Brownian motion of the AF647 dye. A fluorescent bead is introduced as a reference marker to correct drift as marked by the green circle. The red dashed circle depicts the positions of the AF647 dye at different time (T0, T1, T2, …, Tn), which shows an irregular path taken by Brownian motion.

During imaging, the DNA strand suffers from drift while undergoing Brownian motion. Fig. 1c shows the position of the AF647 dye after drift correction. Supposing the drift occur during a time interval between T0 and T1' as indicated by the black solid arrow in Fig. 1c, drift compensation corrects the position of the bead back to its original position at T0. However, for the DNA strand, the position after drift compensation would be a new position (marked as T1) instead of the position at T0, as a result of Brownian motion. A series of positions after drift correction would show the trajectory of random walk in Brownian motion.

Taking the localization error into consideration, if the tether length of the DNA strand is too short, the dynamic of Brownian motion with small amplitude would be difficult to be extracted from the localization dataset.

Calculation of z-score of displacement between localizations from adjacent frames

The raw data of STORM are obtained by identifying and fitting single fluorescent spots, which generates a "localization list" that contains spatial coordinates, frame number. We define each localization of the same molecule as $Loc_i(x_i, y_i, f_i), i = 1, 2, 3, \dots, N$, where N is the total number of localizations. The spread of the localizations follows a gaussian distribution.

We define the displacement between two localizations in adjacent frames as d_1, which can be calculated as

$$d_1 = \sqrt{(x_{i+1} - x_i)^2 + (y_{i+1} - y_i)^2} \text{ , if } f_{i+1} - f_i = 1. \quad (1)$$

Similarly, the displacement between two localizations in random frames is defined as,

$$d_r = \sqrt{(x_i - x_j)^2 + (y_i - y_j)^2}, i, j \in \{Loc\} \tag{2}$$

To establish statistical significance, we sampled randomly from the data set $\{Loc\}$ with the same number of d_1 to get a series of d_r. The mean of both are calculated by

$$\overline{d_1} = mean(d_{1i}) = \frac{1}{L}\sum_{i=1}^{L} d_{1i} \tag{3}$$

$$\overline{d_r} = mean(d_{ri}) = \frac{1}{L}\sum_{i=1}^{L} d_{ri} \tag{4}$$

The sampling is repeated 5000 times to get a series of $\overline{d_r}$, the histogram of which should follows Gaussian distribution according to Central-Limit Theorem. To calculate the statistical difference between d_1 and d_r, we define the z-score of d_1 as

$$z_1 = \frac{\overline{d_1} - mean(\overline{d_{rn}})}{std(\overline{d_{rn}})} \tag{5}$$

The z-score defines how many standard deviations between the adjacent displacement and the random displacement. A negative z-score indicates the $\overline{d_1}$ is below the mean of $\overline{d_r}$.

Note that the position measurement in SMLM can be treated as a random process, as long as the molecule is static or drift is completely corrected, the displacement between two localizations in adjacent frames and that between two random frames should have no statistically significant difference. However, for Brownian motion or drift motion, since the value of displacement should increase with its time interval, which gives a negative z-score that will distinctly deviate from zero.

Using z-score to analyze molecule motion in STORM imaging

In our experiment, the z-scores before and after drift correction are both calculated for 2108 molecules (DNA strands). It is found that the z-scores of most molecules situated near the peak of -2.5 before correction, while the peak shifted to -0.5 after correction, as presented in the histogram plot in Figs. 2A-B. This shows that drift correction is effective for most molecules. After drift correction, the statistical difference between the displacement between two adjacent frames and that between random frames is small for these molecules. However, it can be clearly seen in Fig. 2B that, while the upper limit of z-scores is around 2, there is a certain number of molecules with z-score smaller than -2 after drift correction as marked by the red box in Fig. 2B. The asymmetry of distribution can be more clearly seen in Fig. 3A.

In Fig. 3A, the uncorrected z-score is plotted against the corrected z-score to better demonstrate the change of z-score before and after drift correction. Two dashed black lines indicate z-score value of +2 and -2. Theoretically, for perfect drift correction, any molecule should be corrected to a z-score around zero, no matter what the value is before correction. In this sense, molecules that have z-score

smaller than -2 after correction should indicate failure of drift correction. This divides the molecules into two groups, one with z-score within the range from -2 to +2 after drift correction, suggesting effective correction, and the other one with z-score smaller than -2.

To study the behaviors of the molecules from the two groups, z-scores at different time lag were calculated. We define the displacement of two localizations separated m frames as,

$$d_m = \sqrt{(x_k - x_i)^2 + (y_k - y_i)^2} \text{ , if } f_k - f_i = m. \tag{6}$$

Accordingly, its z-score from Eq. (5) can be revised as

$$z_m = \frac{\overline{d_m} - mean(\overline{d_{rn}})}{std(\overline{d_{rn}})} \tag{7}$$

Fig. 3B-C give the curves of z_m of two molecules from the two different groups at different time lag m, one with $z_1 = 0.06$ (Fig. 3B) and the other one with z_1 =*-3.3687* (Fig. 3C). The curve in Fig. 3B shows random fluctuation around zero, independent of the time lag, suggesting no statistical difference of the displacements. Quite differently, the curve in Fig. 3C shows that the z-score firstly increases with time lag, then reaches a saturation value.

To further show that molecules from the same group have similar behaviors as Fig. 3B-C, all molecules are calculated and plotted in Fig. 4A-B. Fig. 4A shows the z-score z_m of all the 1913 molecules with z_1 ranging from -2 to 2, at different time lag m. Similar to Fig. 3B, the z-scores randomly distributed around zero, independent of time lag. Average of the 1913 molecules was shown in Fig. 4C with errorbar indicating the standard deviation. Fig. 4B displays the z-score z_m of all the 182 molecules with z_1 smaller than -2, at different time lag m. Average of the 182 molecules was depicted in Fig. 4D. Similar to Fig. 3C, the z-score exhibits saturation behavior, which can be fitted by a saturation function $y(x) = y_0 - p_1 exp(-p_2 x)$ with $p_1 = 2.827$, $p_2 = 0.3444$ and $y_0 = -0.3791$ (red line). The curve firstly increases with time lag, indicating that as time increases, the mean of the displacement increases. This is in close analogy to the Brownian motion, where the mean squared distance grows in proportion to the duration of the motion. After a certain time lag, the z-score saturates. This time lag should correspond to the time required for the dye to explore the domain within which it is confined by the DNA tether. When the time lag is larger than the saturation time, the displacement is restricted, leading to a mean displacement $\overline{d_m}$ no different with its randomly sampled counterpart $\overline{d_{rn}}$. Clearly in this regard, the z-score should approximate zero. Yet in the experimental data shown in Fig. 4D, the saturated z-score is fitted as -0.3791. We speculated this discrepancy resulting from inadequate drift correction, which adds slight increment to displacement at large time lag.

Brownian motion simulation

To further confirm our speculations, a 2D Brownian motion confined to a circular disc is performed. We used a constant time interval Δt between frames. Disregarding the localization uncertainty of each frame, if positions could be recorded instantaneously, the position recorded at each frame will be,

$$x_n = \sum_{i=1}^{n} \sqrt{2D\Delta t} \cdot randn(1, N) \tag{8}$$

$$y_n = \sum_{i=1}^{n} \sqrt{2D\Delta t} \cdot randn(1, N) \tag{9}$$

Here, D is the diffusion constant and N is the number of frames that collected. The $randn(1, N)$ generates a 1-by-N array of random numbers from the standard normal distribution.

Since the finite length of the DNA strand, we set an upper limit to the scalar distance $R_n = \sqrt{x_n^2 + y_n^2} < R_0$.

In our simulation, we set $\sqrt{2D\Delta t} = 10.3537\, nm$, $R_0 = 10\, nm$, $N = 8000$. Fig. 5a shows the simulated z-score changing with different time lag. The data is fitted by a saturation function $y(x) = y_0 - p_1 exp(-p_2 x)$ with $p_1 = 5.701$, $p_2 = 0.7497$ and $y_0 = 0.1046$ (black solid line). A distinct deviation from the experimental data in Fig. 4d is that, the maximum z-score in the simulation is close to zero in simulation, while it is around -0.3791 in experiment. The deviation from zero in the experiment might suggest drift correction residual.

To confirm this, a linear term is added to the position coordinates,

$$x_n' = x_n + kn \tag{10}$$

$$y_n' = x_n + kn \tag{11}$$

In our simulation, we set $k = 0.02$. The simulated z-score with different time lag is plotted in Fig. 5b and fitted by a saturation function $y(x) = y_0 - p_1 exp(-p_2 x)$ with $p_1 = 3.019$, $p_2 = 0.292$ and $y_0 = -0.52$ (black solid line). We can see that this simulation result is in better agreement with our experimental result.

Influence of Brownian motion on localization precision

The experimental localization precision is calculated as the standard deviation of the positions of multiple molecules overlaid in their position center. The localization precision of two groups of molecules are calculated. In the first group, we calculated the positions of 722 molecules with $-0.5 < z_1 < 0.5$. The standard deviation is 7.9582 nm in the x-direction and 7.4179 nm in the y-direction. In the second group, 182 molecules with $z_1 < -2$ are calculated, yielding a standard deviation of 12.9665 nm in the x-direction and 11.1103 nm in the y-direction. The result reveals deterioration of localization precision for Brownian motion.

Potential ways to suppress Brownian motion including cooling using water or semiconductor cooler. But additional vibration might be introduced during the cooling process. DNA probes with shorter length would have smaller amplitude of Brownian motion theoretically.

Conclusion

The localization precision is a crucial and important parameter for single-molecule localization microscopy (SMLM) and directly influences the achievable spatial resolution. We show that the localization precision depends not only on the photon number, shot noise and background noise, but also on the amplitude of Brownian motion of the fluorescent probe. We developed a statistical method to extract Brownian motion from the trajectory of the localizations of single molecule.

Materials and Methods

System:

A STORM system based on an inverted optical microscope (IX-71, Olympus) with a 100x oil immersion objective lens (Olympus) was used for the nano-imaging as previously described (22). Astigmatism imaging method was adopted for 3D-STORM, in which a weak cylindrical lens (1 m focal length) was introduced into the imaging path. A 641 nm laser (CUBE 640–100C;Coherent) was used to excite fluorescence and switch Alexa-647 to the dark state. The illumination used the highly inclined and laminated optical sheet (HILO) configuration (23). The laser power densities were approximately 1.45 kW/cm^2 for the 641 nm laser unless otherwise indicated. A dichroic mirror (ZT647rdc, Chroma) was used to separate the fluorescence from the laser and a band-pass filter (FF01-676/37, Semrock) on the imaging path was used to filter the fluorescence. Raw images of the fluorescent signals in each nuclear field were acquired with an EMCCD (DU-897U-CV0, Andor) at 33 Hz for 8000 frames. To avoid focal drift, an anti-drift system was used to sustain the focal position within 10 nm during image processing (24).

Buffer:

A standard STORM imaging buffer containing 50Mm Tris (pH 8.0), 10mM NaCl,1% b-mercaptoethanol (v/v), 10% glucose (w/v), 0.5 mg/mL glucose oxidase (G2133, Sigma), and 40mg/mL catalase (C30, Sigma) (25-26) was used.

Label Protocal:

Each coverslip was incubated at room temperature with 25nM Alexa-647-conjugated oligonucleotides (each 18 nt oligonucleotide labeled with one Alexa-647 at its 3' end) for 8 min and then incubated with 0.2 μm red fluorescent microspheres (F8810, Thermo Fisher) as fiducial markers to correct for sample drift in the x-y plane during imaging.

Method:

For imaging data analysis, a freely available plugin for Image J named Thunderstorm was applied to analyze raw images. The precise localization data of single fluorescent molecules obtained from the fits.

Acknowledgments

This work was supported by Shenzhen Science and Technology Planning Project (JCYJ20170817095211560).

References

1. Rust M J, Bates M, Zhuang X. Sub-diffraction-limit imaging by stochastic optical reconstruction microscopy (STORM)[J]. Nature methods, 2006, 3(10): 793-796.
2. Betzig E, Patterson G H, Sougrat R, et al. Imaging intracellular fluorescent proteins at nanometer resolution[J]. Science, 2006, 313(5793): 1642-1645.
3. Jungmann R, Avendaño M S, Woehrstein J B, et al. Multiplexed 3D cellular super-resolution imaging with DNA-PAINT and Exchange-PAINT[J]. Nature methods, 2014, 11(3): 313-318.
4. Balzarotti F, Eilers Y, Gwosch K C, et al. Nanometer resolution imaging and tracking of fluorescent molecules with minimal photon fluxes[J]. Science, 2017, 355(6325): 606-612.
5. Gwosch K C, Pape J K, Balzarotti F, et al. MINFLUX nanoscopy delivers 3D multicolor nanometer resolution in cells[J]. Nature methods, 2020, 17(2): 217-224.
6. Schmidt R, Weihs T, Wurm C A, et al. MINFLUX nanometer-scale 3D imaging and microsecond-range tracking on a common fluorescence microscope[J]. Nature Communications, 2021, 12(1): 1-12.
7. Van de Linde S, Löschberger A, Klein T, et al. Direct stochastic optical reconstruction microscopy with standard fluorescent probes[J]. Nature protocols, 2011, 6(7): 991.
8. Huang B, Wang W, Bates M, et al. Three-dimensional super-resolution imaging by stochastic optical reconstruction microscopy[J]. Science, 2008, 319(5864): 810-813.
9. Huang B, Babcock H, Zhuang X. Breaking the diffraction barrier: super-resolution imaging of cells[J]. Cell, 2010, 143(7): 1047-1058.
10. Thompson R E, Larson D R, Webb W W. Precise nanometer localization analysis for individual fluorescent probes[J]. Biophysical journal, 2002, 82(5): 2775-2783.
11. Deschout H, Zanacchi F C, Mlodzianoski M, et al. Precisely and accurately localizing single emitters in fluorescence microscopy[J]. Nature methods, 2014, 11(3): 253.
12. Bon P, Bourg N, Lécart S, et al. Three-dimensional nanometre localization of nanoparticles to enhance super-resolution microscopy[J]. Nature communications, 2015, 6(1): 1-8.
13. Lee S H, Baday M, Tjioe M, et al. Using fixed fiduciary markers for stage drift correction[J]. Optics express, 2012, 20(11): 12177-12183.
14. Wang Y, Schnitzbauer J, Hu Z, et al. Localization events-based sample drift correction for localization microscopy with redundant cross-correlation algorithm[J]. Optics express, 2014, 22(13): 15982-15991.
15. Mlodzianoski M J, Schreiner J M, Callahan S P, et al. Sample drift correction in 3D fluorescence photoactivation localization microscopy[J]. Optics express, 2011, 19(16): 15009-15019.
16. Deschout H, Neyts K, Braeckmans K. The influence of movement on the localization precision of sub‐resolution particles in fluorescence microscopy[J]. Journal of biophotonics, 2012, 5(1): 97-109.
17. Michalet X. Mean square displacement analysis of single-particle trajectories with localization error: Brownian motion in an isotropic medium[J]. Physical Review E, 2010, 82(4): 041914.
18. Markaki Y, Smeets D, Fiedler S, et al. The potential of 3D‐FISH and super‐resolution structured illumination microscopy for studies of 3D nuclear architecture: 3D structured illumination microscopy of defined chromosomal structures visualized by 3D (immuno)‐FISH opens new perspectives for studies of nuclear architecture[J]. Bioessays, 2012, 34(5):

412-426.
19. Wang S, Su J H, Beliveau B J, et al. Spatial organization of chromatin domains and compartments in single chromosomes[J]. Science, 2016, 353(6299): 598-602.
20. Doksani Y, Wu J Y, de Lange T, et al. Super-resolution fluorescence imaging of telomeres reveals TRF2-dependent T-loop formation[J]. Cell, 2013, 155(2): 345-356.
21. Beliveau B J, Boettiger A N, Avendaño M S, et al. Single-molecule super-resolution imaging of chromosomes and in situ haplotype visualization using Oligopaint FISH probes[J]. Nature communications, 2015, 6(1): 1-13.
22. Ni Y, Cao B, Ma T, et al. Super-resolution imaging of a 2.5 kb non-repetitive DNA in situ in the nuclear genome using molecular beacon probes[J]. Elife, 2017, 6: e21660.
23. Tokunaga M, Imamoto N, Sakata-Sogawa K. Highly inclined thin illumination enables clear single-molecule imaging in cells[J]. Nature methods, 2008, 5(2): 159-161.
24. Ying-Dong H, Bo C, Bin Y, et al. A real-time axial active anti-drift device with high-precision[J]. 2015.
25. Dempsey G T, Vaughan J C, Chen K H, et al. Evaluation of fluorophores for optimal performance in localization-based super-resolution imaging[J]. Nature methods, 2011, 8(12): 1027.
26. Olivier N, Keller D, Gönczy P, et al. Resolution doubling in 3D-STORM imaging through improved buffers[J]. PloS one, 2013, 8(7): e69004.

Figures and Tables

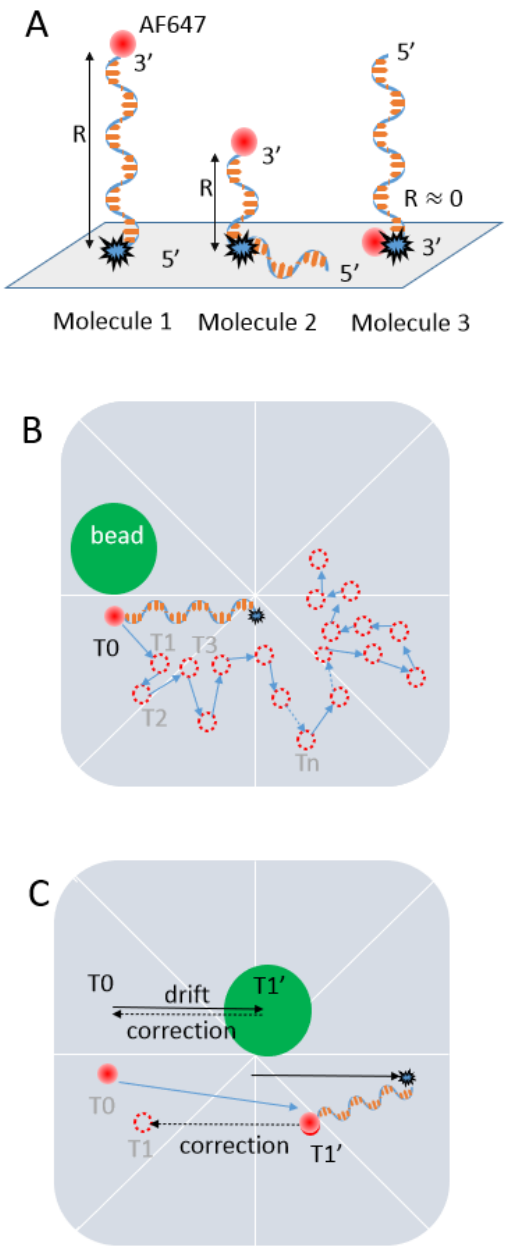

Figure 1. Illustration of Brownian motion of fluorescent DNA probes in STORM imaging. (A) Fluorescent DNA probes with various tether length. (B) Illustration of Brownian motion of a DNA probe in imaging buffer. (C) Brownian motion cannot be corrected by drift correction.

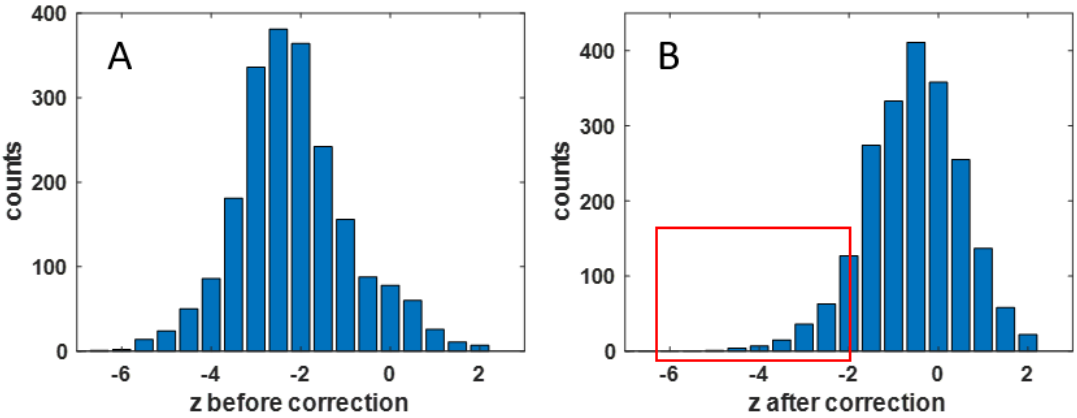

Figure 2. The histogram of z-score before correction (A) and after correction (B).

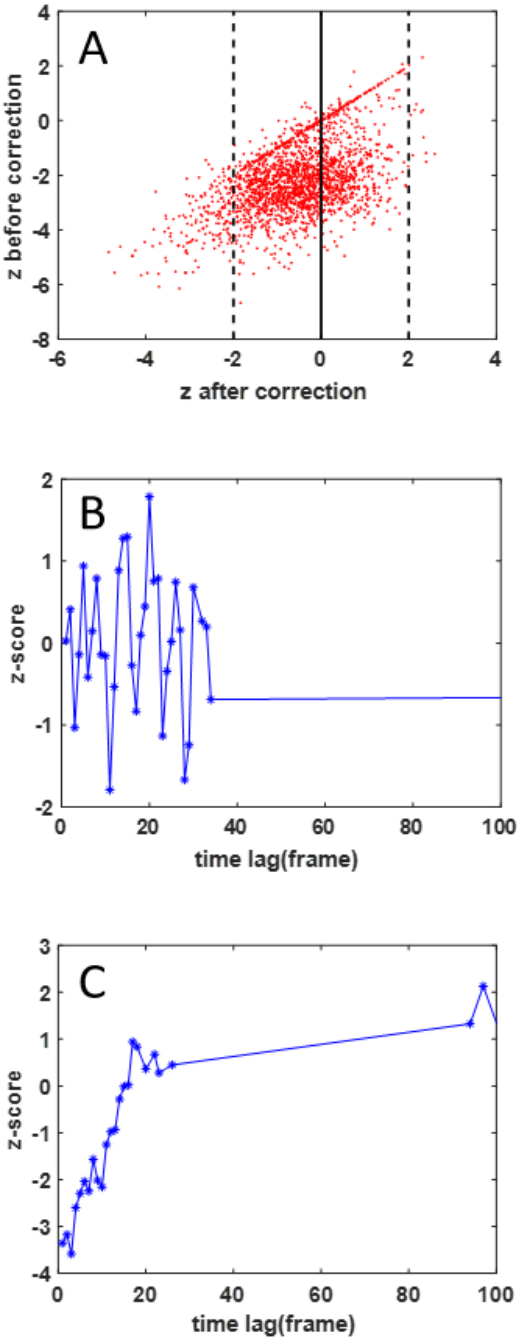

Figure 3. (A) A plot of the z-score before and after correction, which shows that some molecules can be corrected to a z-score around zero, but some molecules still have a large negative z-score after correction. The black solid line indicates z-score of zero after correction. The black dashed line represents a z-score of -2 and 2 after correction. (B) the z-score after correction of the molecules near the black solid line in (A) with different time lag. (C) the z-score after correction of the molecules at the far negative regime of (A) with different time lag.

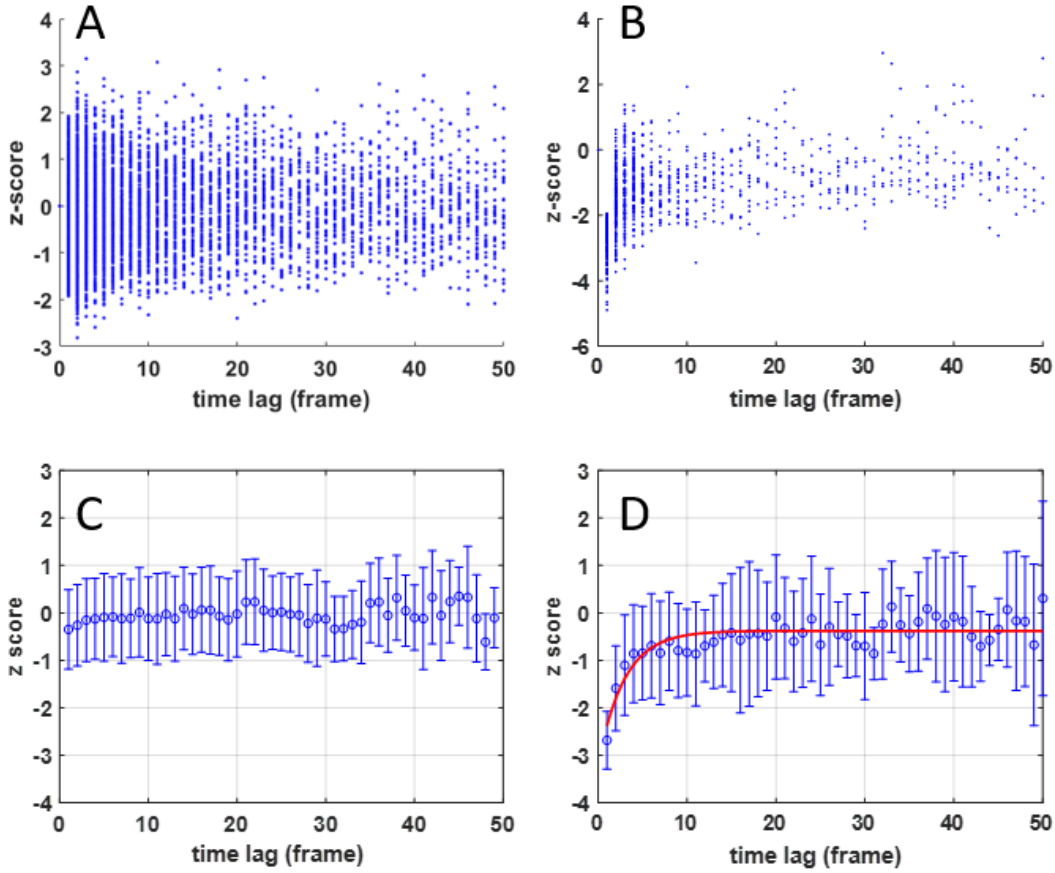

Figure 4. (A) The time-dependence of z-scores of 1913 molecules with z_1 ranging from -2 to 2. (B) The time-dependence of z-scores of 182 molecules with z_1 smaller than -2. (C) the z-scores averaged by the 1913 molecules in (A) at different time lag. (D) the z-scores averaged by the 182 molecules in (B) at different time lag.

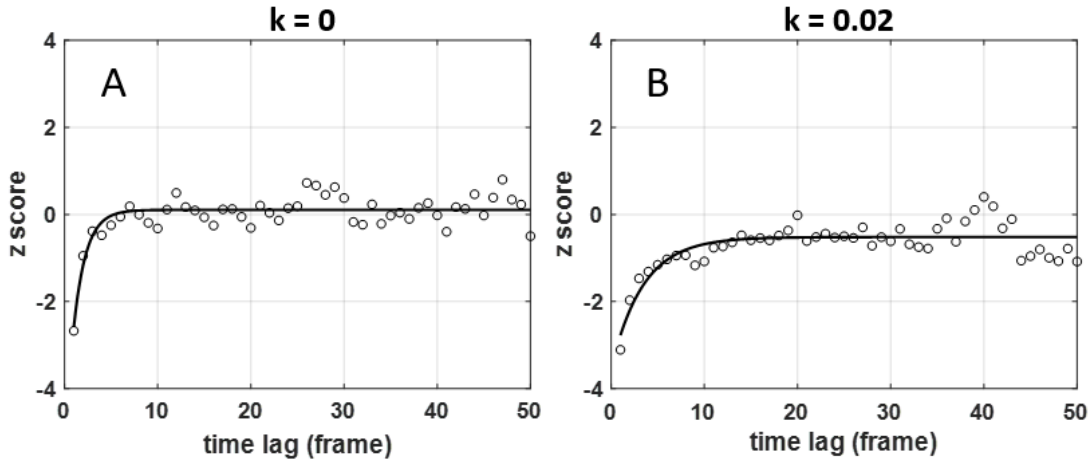

Figure 5. Simulated z-scores (black circle) with $z_1 < -2$ at different time lag and the fitted saturation function (black line) without (A) and with (B) drift correction residual.